Quantum-size effects in the loss function of Pb(111) thin films: An *ab initio* study

X. Zubizarreta,[1,2,3] E. V. Chulkov,[2,3,4] I. P. Chernov,[5] A. S. Vasenko,[6] I. Aldazabal,[4] and V. M. Silkin[2,3,7]

[1]*IMPMC, Université Pierre et Marie Curie (UPMC), Paris, France*

[2]*Donostia International Physics Center (DIPC), P. de Manuel Lardizabal 4, 20018 San Sebastián/Donostia, Spain*

[3]*Departamento de Física de Materiales, Facultad de Ciencias Químicas, Universidad del País Vasco/Euskal Herriko Unibertsitatea, Apdo. 1072, 20080 San Sebastián/Donostia, Spain*

[4]*Centro de Física de Materiales CFM - Materials Physics Center MPC, Centro Mixto CSIC-UPV/EHU, P. de Manuel Lardizabal 5, 20018 San Sebastián/Donostia, Spain*

[5]*Tomsk Polytechnical University, pr. Lenina 30, 634050 Tomsk, Russia*

[6]*National Research University Higher School of Economics, 101000 Moscow, Russia*

[7]*IKERBASQUE, Basque Foundation for Science, 48011 Bilbao, Spain*

(Received 22 September 2016; revised manuscript received 12 May 2017; published 5 June 2017)

A theoretical study of collective electronic excitations in free-standing Pb(111) thin films consisting of 1–5 monolayers (MLs) and a 21-ML film is presented. The calculations are carried out applying the linear response theory, with full inclusion of the electron band structure by means of a first-principles pseudopotential approach in a supercell scheme. In the case of the thickest film, we find that, due to strong bulklike interband transitions, at the Pb(111) surface there are two surface modes. For thin films, a mechanism of transformation of these modes to the symmetric and antisymmetric classic hybrid plasmons is investigated. Pronounced quantum-size effects on plasmon modes of the thinnest films are found. Strong influence of the band structure on dispersion and lifetime of such modes is demonstrated. The present results are in good agreement with available experimental data for a Pb surface and thin films.

DOI: 10.1103/PhysRevB.95.235405

I. INTRODUCTION

In thin metallic films, spatial confinement in the direction perpendicular to the film plane gives rise to the quantization of the electronic states. As a result of appearance of the so-called quantum-well states (QWS) [1], the properties of metallic films might strongly depend on their thickness. This dependence is a purely quantum phenomena known as quantum-size effect (QSE), which was revealed, for instance, in thin lead films, in the layer-by-layer growth [2], attributed to the modulation of the electron density of states (DOS) at the Fermi level (E_F). This modulation causes oscillations with the thickness in the superconducting critical temperature and electron-phonon coupling [3–5], interlayer distances [6,7], island height distributions [8], zone-center phonon frequencies [6,9,10], electronic transport [11], photoemission properties [12], work functions [13], quasiparticle lifetimes [5,14,15], and plasmonic modes [16]. Also, superconductivity [17,18], switching between one- and two-dimensional conductance properties [19–22], and phase transitions [23] were observed in a single lead monolayer (ML) absorbed on silicon. Thus lead films have become an important model system for exploring electronic and structural properties of metals on the nanoscale [24,25].

However, to the best of our knowledge, there are few experimental studies of the surface response and plasmonic properties of thin Pb slabs [26–30], and no theoretical work. Thus the aim of the present work is a systematic study of the surface energy-loss function of Pb(111) films with varying thickness, starting from a single monolayer case up to the 5 MLs film. For comparison we also perform calculations for a 21-ML slab thus simulating a semi-infinite Pb(111) surface.

An approximate description of thin film plasmons can be given by a solution of the Maxwell equations for the proper geometry [31]. It leads to the coupling between the classical surface plasmons of two different surfaces of the film. The resulting coupled modes of the Drude thin film disperse as [31–33]

$$\omega_{\pm}(q_{\parallel}) = \frac{\omega_p}{\sqrt{2}}(1 \pm e^{-q_{\parallel}L})^{1/2}, \tag{1}$$

where ω_p is the bulk plasmon frequency, which for a free-electron gas is given by $\omega_p = \sqrt{4\pi n/m^*}$ with n being the electron density and m^* the electron effective mass, which in terms of the density parameter r_s standing for the average interelectron distance reads as $\omega_p = \sqrt{3/r_s^3\, m^*}$. As follows from Eq. (1), the energy splitting between the modes depends on the film thickness L and the in-plane momentum transfer $q_{\parallel}$. The low-energy mode ω_- corresponds to a symmetric induced charge profile in the direction perpendicular to the film plane, whereas the high-energy mode ω_+ corresponds to an asymmetric one [34]. As L increases, the coupling between the two modes decreases. In the $L \gg 1/q_{\parallel}$ limit, two film modes are spatially decoupled and two classical surface plasmons of frequency $\omega_p/\sqrt{2}$ at each surface are retrieved. However, this simple model, providing a general picture, does not describe, for instance, how upon $L \to 0$ these two modes of a finite-thick film evolve into a single mode in a pure two-dimensional electron system [35]. Moreover, it ignores the details of the film electronic structure which may be a serious drawback since the realistic electronic structure has been shown to strongly affect the surface response function [36–43]. Additionally, a more detailed classical model showed the dependence of the surface plasmon dispersion on the microscopic details of the surface electronic density profile [44,45].

On a quantitative level, the jellium model [46] has been used to study the quantum-mechanical electrodynamical

response of metal and semiconductor slabs [34,47–60] and nanoparticles [61–67] gaining basic insight into the nature of electronic excitations in such systems and corresponding electric field distribution. As an example, Yuan and Gao have shown [34], using the jellium model with the electron density corresponding to Ag, the disappearance of the antisymmetric mode ω_+ at $q_\parallel \to 0$ when the film thickness is comparable to the Fermi wavelength. Instead, a few discrete interband peaks were found [34].

A more precise description of the electron band structure in the direction perpendicular to the film plane [68], allowing to describe the surface states which are missing in a jellium model, was recently used to study new collective electronic excitations at metal surfaces [69,70] and thin metal films [71]. However, this recipe [68] of the improved one-dimensional potential can not give a satisfactory description of the electronic structure of Pb(111) films since in Pb the band structure strongly influences the excitation spectrum [72–74]. At the surface, the properties of the surface plasmon indeed are very sensitive to the electronic structure details. Thus its dispersion can be strongly affected as it occurs on silver surfaces where the interband transitions involving valence 4*d* electrons drastically shift downward the surface plasmon energy [41,75]. Impact of this kind of transitions is even more dramatic in copper where they completely suppress the surface plasmon [41]. Moreover, the band structure almost entirely determines the surface plasmon lifetime at small momentum transfers [32].

In order to fully take into consideration the surface electronic band structure, new first-principles calculation methods have recently been developed. Such an approach has become feasible for the description of collective electronic excitations in films and at surfaces. It was applied to simple [36,76] and noble [41,77] metals and semiconductor [39] clean surfaces, graphene [78–89], and adsorbate-covered surfaces [90,91]. These calculations confirmed that the energy dispersion of plasmons in real systems can be described in close agreement with the experimental findings. Moreover, these calculations can describe the lifetime of such excitations, which is of a paramount importance in the field of plasmonics, since it determines the plasmon propagation length.

In the present work, a first-principles approach is used to study the dielectric response of Pb(111) films. Using an *ab initio* calculation scheme makes possible to study anisotropy effects, which are missing in jellium models or even in a more sophisticated model potential approach [68], as they assume an in-plane free-electron-like behavior.

In this work, we show that the surface plasmon modes of the Pb films follow qualitatively the classical dispersion relation of Eq. (1). However, for the thinnest slabs, notable QSE are found. Moreover, a strong impact of the realistic band structure on the excitation spectrum of Pb surface and thin films is observed. Thus, in addition to the dominating surface plasmon mode, a dispersionless mode is found in the surface loss spectrum at energies $\omega \simeq 7$ eV. A mechanism of transformation of the surface plasmons into two hybridized slab modes is revealed.

The rest of the paper is organized as follows. In Sec. II, the details of the *ab initio* calculation of the surface loss function are given. In Sec. III, the calculated ground state electronic structures of all considered films are presented. In Sec. IV, the surface loss function results are analyzed in detail. Finally, the conclusions are drawn in Sec. V. Unless otherwise stated, atomic units are used throughout, i.e., $e^2 = \hbar = m_e = 1$.

II. CALCULATION METHOD

When a perturbing electric charge is located far from the film the differential cross section for its scattering with energy ω and in-plane momentum transfer $\mathbf{q}_\parallel$ is proportional to the imaginary part of the surface response function $g(\mathbf{q}_\parallel,\omega)$ defined as [92]

$$g(\mathbf{q}_\parallel,\omega) = -\frac{2\pi}{q_\parallel}\int d\mathbf{r}\int d\mathbf{r}'\,\chi(\mathbf{r},\mathbf{r}',\omega)e^{q_\parallel(z+z')}e^{i\mathbf{q}_\parallel(\mathbf{r}_\parallel-\mathbf{r}'_\parallel)}, \quad (2)$$

which depends on the film electronic properties only. Here, the z axis is pointing in a direction perpendicular to the surface, i.e., $\mathbf{r} \equiv \{\mathbf{r}_\parallel, z\}$, and ($q_\parallel \equiv |\mathbf{q}_\parallel|$). The surface response function is relevant in the description of surface collective excitations measured in electron energy-loss experiments performed in a reflection geometry [32,93]. Here, $\chi(\mathbf{r},\mathbf{r}',\omega)$ is the density response function of an interacting electron system that determines, within linear response theory, the electron density $n^{\rm ind}(\mathbf{r},\omega)$ induced in the system by an external potential $V^{\rm ext}(\mathbf{r},\omega)$ according to

$$n^{\rm ind}(\mathbf{r},\omega) = \int d\mathbf{r}'\,\chi(\mathbf{r},\mathbf{r}',\omega)V^{\rm ext}(\mathbf{r}',\omega). \quad (3)$$

The collective electronic excitations in thin films then can be traced to the peaks in the surface loss function defined as an imaginary part of g, $\mathrm{Im}[g(\mathbf{q}_\parallel,\omega)]$.

In the framework of time-dependent density functional theory [94,95], χ is a solution of the integral equation

$$\chi(\mathbf{r},\mathbf{r}',\omega) = \chi^o(\mathbf{r},\mathbf{r}',\omega) + \int d\mathbf{r}_1\int d\mathbf{r}_2\chi^o(\mathbf{r},\mathbf{r}_1,\omega) \times [v_c(\mathbf{r}_1,\mathbf{r}_2) + K_{\rm XC}(\mathbf{r}_1,\mathbf{r}_2,\omega)]\chi(\mathbf{r}_2,\mathbf{r}',\omega) \quad (4)$$

with χ^o being the response function (polarizability) of the noninteracting Kohn-Sham electrons. In Eq. (4), v_c stands for the bare Coulomb potential and $K_{\rm XC}$ accounts for the exchange-correlation (XC) effects. In the present work, we use the random-phase approximation (RPA) where $K_{\rm XC}$ is set to zero, i.e., the dynamical short-range exchange-correlation effects are ignored. Previous studies of collective excitations at surfaces [36,96–98] and in bulk [99,100] of many metallic systems suggest that XC effects should have little impact on the excitation spectra at small $q_\parallel$'s. Its role in determining the dispersion and lifetime of plasmonic modes may become notable with increasing $q_\parallel$ [96,101]. However, due to a relatively low effective electron density parameter r_s and, as was shown in previous calculations for bulk Pb collective excitations [73,74,102], we do not expect significant changes in the results for Pb slabs presented here.

For a description of the electronic structure and excitation spectra of a free-standing film, we employ a three-dimensional model considering a repeated slab geometry with the Pb(111) slabs of certain thickness separated by vacuum intervals. In this case, having a periodic system in all three directions, the χ^o response function can be expressed as a matrix in the basis of the reciprocal space lattice vectors $\mathbf{G}$'s. As a consequence, Eq. (4) becomes a matrix equation. Then, once the ground

state has been obtained, the starting point of the calculation of the surface response function is the evaluation of the matrix elements of the response function of noninteracting electrons:

$$\chi^{o}_{\mathbf{G}\mathbf{G}'}(\mathbf{q}_{\parallel},\omega) = \frac{2}{S}\sum_{\mathbf{k}_{\parallel}}^{\mathrm{SBZ}}\sum_{n}^{\mathrm{occ}}\sum_{n'}^{\mathrm{unocc}}\frac{f_{n\mathbf{k}_{\parallel}} - f_{n'\mathbf{k}_{\parallel}+\mathbf{q}_{\parallel}}}{E_{n\mathbf{k}_{\parallel}} - E_{n'\mathbf{k}_{\parallel}+\mathbf{q}_{\parallel}} + (\omega + i\eta)} \times \langle\phi_{n\mathbf{k}_{\parallel}}|e^{-i(\mathbf{q}_{\parallel}+\mathbf{G})\mathbf{r}}|\phi_{n'\mathbf{k}_{\parallel}+\mathbf{q}_{\parallel}}\rangle\langle\phi_{n'\mathbf{k}_{\parallel}+\mathbf{q}_{\parallel}}|e^{i(\mathbf{q}_{\parallel}+\mathbf{G}')\mathbf{r}}|\phi_{n\mathbf{k}_{\parallel}}\rangle, \quad (5)$$

where S is normalization constant, n (n') is an occupied (unoccupied) band index, $\mathbf{k}_{\parallel}$ is the two-dimensional surface Brillouin zone (SBZ) vector, $f_{n\mathbf{k}_{\parallel}}$ are Fermi factors, and $E_{n\mathbf{k}_{\parallel}}$ ($\phi_{n\mathbf{k}_{\parallel}}$) are the Kohn-Sham energies (wave functions). In order to speed up the χ^{o} calculations, we follow Refs. [99,103], where the spectral function is calculated first. Then from its knowledge the imaginary and real parts of $\chi^{o}_{\mathbf{G}\mathbf{G}'}$ are obtained. Finally, the expression for the surface response function in the case of a periodically repeated slab reads [36]

$$g(\mathbf{q}_{\parallel},\omega) = -\frac{2\pi}{q_{\parallel}}\int dz\int dz'\,\chi_{\mathbf{G}_{\parallel}=\mathbf{G}'_{\parallel}=0}(z,z',\mathbf{q}_{\parallel},\omega)e^{q_{\parallel}(z+z')}. \quad (6)$$

Even though only the $\mathbf{G}_{\parallel} = \mathbf{G}'_{\parallel} = 0$ matrix elements of $\chi_{\mathbf{G}\mathbf{G}'}$ enter Eq. (6), full three-dimensional (3D) nature of the polarizability is implicity taken into account via the evaluation of Eq. (4) as a matrix equation.

Furthermore, in order to save computational time, $\chi^{o}_{\mathbf{G}\mathbf{G}'}$ has been calculated retaining only $\mathbf{G} = (0,0,G_z)$ reciprocal space vectors. Physically, this means that the lateral crystal local field effects were neglected. This approach was already found to give indistinguishable results compared with the calculations carried out using the full 3D **G**'s for some metal surfaces [36]. All important 3D effects are included in the evaluation of $\chi^{o}_{\mathbf{G}\mathbf{G}'}$ through the use of the fully 3D Bloch functions and their respective one-electron energies.

In the present work, the Pb(111) films are represented by free-standing slabs infinite in the xy plane and periodically repeated in the z direction, separated by a vacuum region whose width was fixed in all cases to be equal to 10 interlayer distances in the z direction. Films are not relaxed, representing ideal cuts of the face-centered cubic bulk Pb in the (111) direction with the bulk experimental lattice parameter of 4.95 Å. Thus, the in-plane lattice parameter is $a = 3.50$ Å and the interlayer distance is $c = 2.86$ Å.

For the density functional theory (DFT) ground-state calculations [104], the electron-ion interaction was represented by a norm-conserving nonlocal pseudopotential [105], and the LDA approximation was chosen for the exchange-correlation potential, with the use of the Perdew-Zunger [106] parametrization of the XC energy of Ceperley and Alder [107]. Well-converged results have been found with a kinetic energy cutoff of ~220 eV, including from ~2200 (1 ML) to ~6600 (21 ML) plane waves in the expansion of the Bloch states.

The calculation of $\chi^{o}_{\mathbf{G}\mathbf{G}'}(\mathbf{q}_{\parallel},\omega)$ was performed employing our own code [108]. Summation over SBZ in Eq. (5) was carried out using a Monkhorst-Pack 240×240 grid of $\mathbf{k}_{\parallel}$ vectors as the hexagonal SBZ sampling with 57600 vectors in the SBZ. All energy bands with energies up to 50 eV above the Fermi level were included in the evaluation of $\chi^{o}_{\mathbf{G}\mathbf{G}'}(\mathbf{q}_{\parallel},\omega)$. The width of the Gaussian replacing the delta function in the evaluation of $\chi^{0}_{\mathbf{G}\mathbf{G}'}(\mathbf{q}_{\parallel},\omega)$ was set to 0.15 eV, a value that gave smooth results while not hiding any feature on the surface loss function of the films. Well converged results were found with the size of the polarizability matrix up to 100 **G** vectors.

An important issue in using a repeated-slab geometry for the description of the plasmonic excitations in thin films is the elimination of the spurious long-range Coulomb interaction between the oscillating charge density in different slabs. For instance, this does not allow us to describe properly a long-wavelength dispersion of a 2D plasmon [109]. Several approaches to solve this problem were proposed. In this work, we follow the receipt proposed by Nazarov [110].

III. ELECTRONIC STRUCTURE

The calculated electronic band structure of Pb(111) films of several thicknesses is shown in Fig. 1. Here one can see how for a N ML thick film, each bulk state energy level is split in N subbands. The subbands below −6 eV are of s character. They are separated by a gap from the $3N$ subbands of p character, which form the Fermi surface of the slabs. As can be seen in Fig. 1, the width of the gap is already fixed as ~2 eV for the 3-ML thick film.

Around the SBZ center ($\overline{\Gamma}$ point), the energy bands show a parabolic free-electron-like dispersion. The p bands around $\overline{\Gamma}$ present a p_z character, while acquiring an increasing $p_{x,y}$ component as they loose their paraboliclike dispersion moving away from $\overline{\Gamma}$ [15]. The p_z states represent the QWS of the Pb(111) films. The inverse of the energy separation of the QWS around E_F is linearly proportional to the film thickness, in good agreement with a previous study [111].

As lead is a heavy element (atomic number 82), a spin-orbit (SO) interaction has notable effects on its energy spectrum. As an example, in bulk Pb, the SO-induced splitting at the bulk Brillouin zone (BZ) center is ~3 eV, and several degeneracies are lifted throughout the bulk BZ [72]. However, the dispersion of energy bands crossing the Fermi level is not altered significantly [72]. In Fig. 1, the band structure for the 1–3-ML thick films is shown with (dash lines) and without (solid lines) the SO coupling included in the Hamiltonian. As can be seen, in thin films, the SO effects around the Fermi level are significant only for a single monolayer, which becomes semimetallic when the SO interaction is switched on, as a result of the lifting of the band crossings existing in the scalar-relativistic case. However, as the slab thickness is increased, the SO effects on the energy bands of Pb(111) films become smaller for slabs as thin as 3 ML (see Fig. 1). As a consequence, SO effects are not expected to affect qualitatively the films surface loss function, except for the Pb(111) monolayer.

IV. RESULTS AND DISCUSSION

A. Jellium model calculations

In order to make connection with previous works on the collective electronic excitations in thin films, we report in Fig. 2 the surface loss function, $\mathrm{Im}[g(\mathbf{q}_{\parallel},\omega)]$, evaluated within a jellium model for six different slabs consisting of 1–5 and 21 MLs. Comparing the loss function in these plots obtained for $r_s = 2.298$ with the results of Yuan and Gao

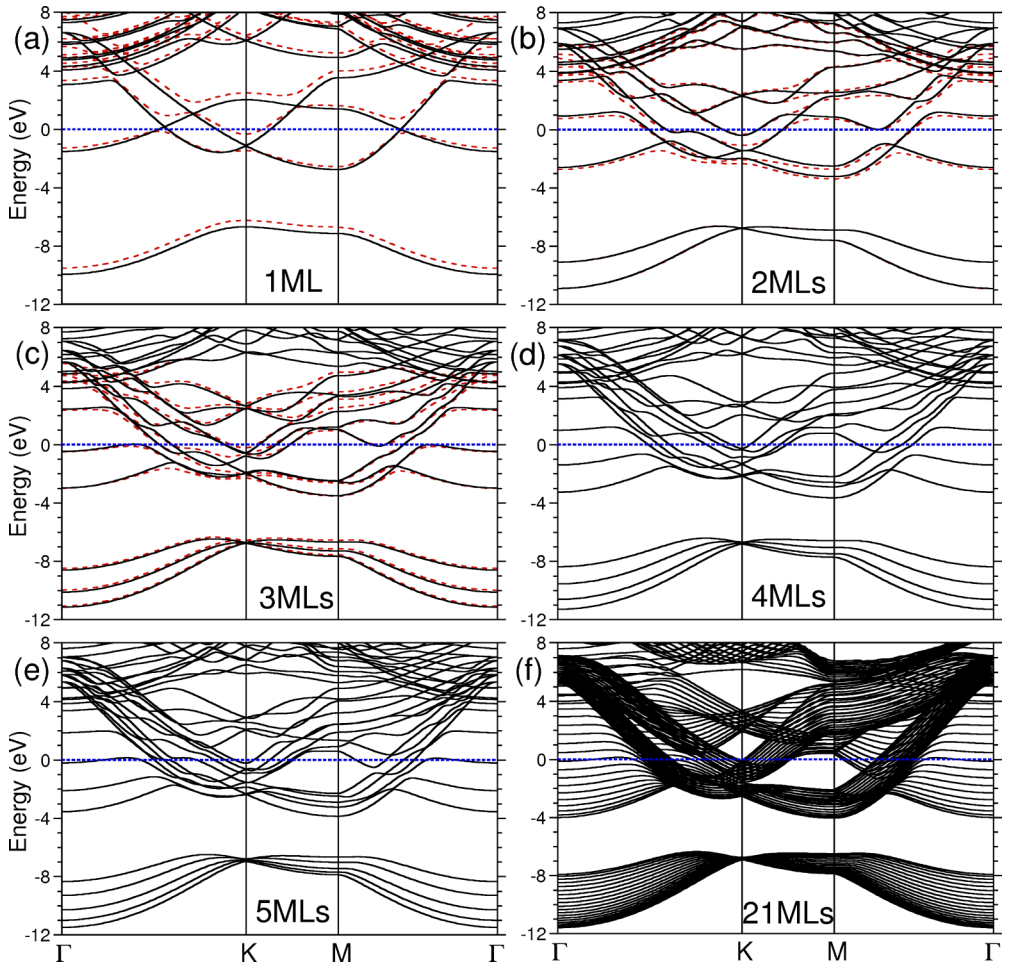

FIG. 1. Band structure of the Pb(111) free-standing films consisting of 1–5 and 21 MLs, calculated without (solid lines) and with (dash lines) spin-orbit (SO) coupling included in the Hamiltonian. In each panel, the horizontal dot line represents the Fermi level position set to zero.

[34] obtained for $r_s = 3$ within the same model one can find a qualitatively similar picture. In particular, at momentum transfer $q_\parallel$ exceeding a certain critical value $q_\parallel^c$, a single peak corresponding to the surface plasmon of a single film surface can be observed for $N \geqslant 2$. Only in the case of a 1-ML slab we do not find a single surface plasmon mode. Instead, two prominent peaks appear at large momentum transfers in Fig. 2(f), which do not merge each other at any momentum.

At intermediate $q_\parallel$'s smaller than $q_\parallel^c$, the loss spectra present two hybridized slab plasmon modes: the lower-energy symmetric mode ω_- and the higher-energy antisymmetric one ω_+. Even in a 1-ML film case, one can discern the peak, corresponding to the ω_+ mode, with energies around 10 eV. Around the same energy such a mode can be clearly observed in 2–5-ML slabs as well. However, in the thinnest slabs, the intensity of this mode is significantly reduced in comparison with that of the symmetric mode. Only in slabs with thickness exceeding four atomic layers the intensities of both these modes become similar.

Finally, at small momentum transfers in thin films, the antisymmetric mode looses its collective character and breaks up in several interband single-particle excitations. Correspondingly, in the surface loss function, the peaks resulting from the discrete interband transitions show up. For instance, in the surface loss function of a single monolayer shown in Fig. 2(f), a manifold of well-resolved single-particle interband peaks is present in a 4–16 eV interval. Upon the thickness increase, the distances between such peaks, as well as their intensities, reduce up to their transformation into a featureless background in thick films. Thus, in Fig. 2(a), one can see that a 21-ML film has sufficient thickness to prevent the appearance of such separate single-particle peaks and the disappearance of an antisymmetric mode at small $q_\parallel$'s. Indeed, the dispersion of the corresponding calculated peak ω_+ closely follows the classical dispersion of Eq. (1) as depicted by the upper solid white line. In contrast, the symmetric mode preserves its collective nature at all momentum transfers as evidenced by the sharpness of the corresponding peak in the calculated loss functions for all films. From the surface loss function of the thick 21-ML film of Fig. 2(a), one can deduce that the surface plasmon $\omega_{\rm sp}$ dispersion has a minimum at $q_\parallel = 0.05$ a.u., i.e., the surface plasmon peak has a negative dispersion at small q's and a positive one at large momenta, in accord to the semi-infinite jellium model prediction [32].

Additionally, in the low-energy part of the spectra of thin films presented in Fig. 2, one can detect a well defined peak with a characteristic soundlike dispersion, i.e., at $q_\parallel = 0$, its energy is zero and the dispersion, denoted as $\omega_{\rm ap}$ in

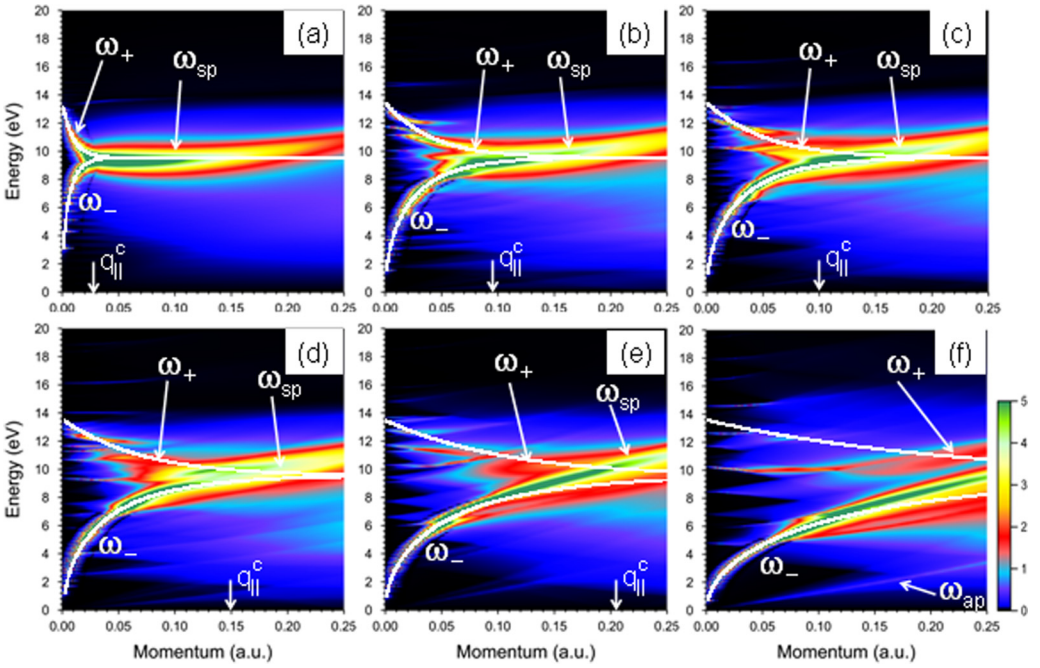

FIG. 2. Surface loss function, Im[$g(\mathbf{q},\omega)$], for (a) 21-, (b) 5-, (c) 4-, (d) 3-, (e) 2-, and (f) 1-ML-thick Pb(111) slabs calculated with a jellium model. Peaks corresponding to the hybrid slab surface ω_- and ω_+ modes, surface plasmon ω_{sp}, and acoustic plasmon ω_{ap} are highlighted by the corresponding symbols. Solid white lines present the dispersion of the ω_- and ω_+ hybrid modes according to Eq. (1) with $\omega_p = 13.53$ eV of the free-electron model. The position of a critical momentum $q_\parallel^c$ showing transition between the slab hybrid modes and the surface plasmon of a single slab surface is shown as well.

Fig. 2(f), is a linear function of the momentum transfer. We identify this mode as an acoustic plasmon (AP). The signature of such a mode in thin films was found in similar jellium calculations previously [71]. Its origin was traced to the existence of more than one energy bands crossing the Fermi level with different Fermi velocities. As a result, the incomplete dynamical screening of the slow carriers in one energy band by the fast carriers in the other leads to the appearance of such a mode with a dispersion slope determined by the Fermi velocity of the slow component. The strength of this AP is maximal in the 1-ML case since only two energy bands are crossing the Fermi level. In general, the number of such plasmons, dispersing with different slopes, should be equal to the number of energy bands crossing the Fermi level minus one. For instance, in the case of the 2-ML film surface loss function shown in Fig. 2(e), one can find two such modes since three energy bands are at the Fermi level. The intensity of the lowest AP mode is significantly stronger than that of the upper mode, which hardly can be discerned in Fig. 2(e). Interestingly, a total intensity of both such modes in the 2-ML film case is significantly smaller than the intensity of a single AP mode in the 1-ML film. This fact can be explained by a mutual interaction of these two modes leading to a partial reduction of spectral weight of each mode. Upon increase of the film thickness, the number of energy bands crossing the Fermi level increases as well. As a result, one might expect that a number of the AP modes should increase as well. However, the mutual destruction of these modes increases as well, which results in an efficient destruction of such modes in the films under study with a number of layers larger than 4.

In order to correctly determine the character of modes corresponding to the peaks found in the surface loss function, it is useful to analyze the spatial distribution of the corresponding oscillating charge. In Fig. 3, we report, as an example, a spatial distribution versus energy of the imaginary part of the charge density induced in a 4-ML film in response to the application of an external potential $V^{\rm ext}(z,\omega) = -2\pi/q_\parallel \cdot e^{q_\parallel z}$ for four values of momentum $q_\parallel$. In the case of small $q_\parallel$ of Fig. 3(a), one can resolve the symmetric ω_{sp}^- slab mode at $\omega = 4$ eV. The symmetric distribution of this charge respective to the slab center clearly indicates its character. At the same momentum at energy $\omega = 12.2$ eV, strong density oscillations, which have an antisymmetric distribution relative to the slab center can be observed as well. These oscillations produce a sharp peak in the loss function of Fig. 2(c) and can be considered as a signature of existence of an antisymmetric mode. However, this mode strongly interacts with the interband transitions as confirmed by the strong variation of density at the nearby energies.

At the intermediate momentum transfer $q_\parallel = 0.041$, the assignment of the symmetric mode in the induced charge density plotted in Fig. 3(b) can be easily revealed at energy of 7 eV. However, even at such large momentum, the antisymmetric mode is still not fully formed. Indeed, in the corresponding energy interval at this momentum there are two strong density oscillations at $\omega = 10$ and 12 eV with an antisymmetric distribution but with different spatial distributions relative to the surface position.

Upon further increase of the momentum, the energy splitting between the symmetric and antisymmetric modes reduces. This approach is accompanied by the formation of a true collective nature of the ω_+ mode. This can be seen

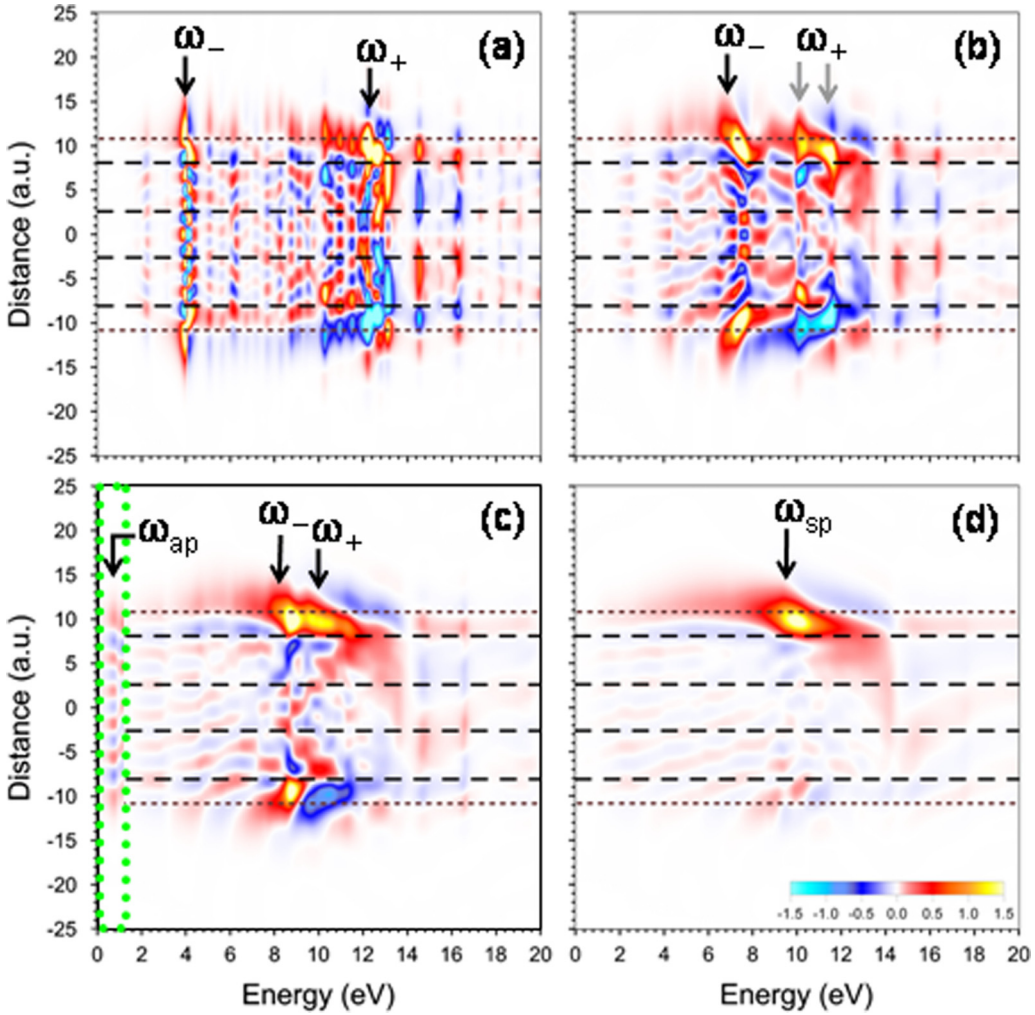

FIG. 3. Imaginary part of the induced density for the 4-ML Pb(111) film obtained from the jellium model calculations is shown as a function of the energy transfer ω and the coordinate z for $q_\parallel$= (a) 0.009, (b) 0.041, (c) 0.078, and (d) 0.160 a.u. Horizontal dot and dash lines mark the jellium slab edges and the atomic layer positions, respectively. Charge oscillations corresponding to the ω_-, ω_+, ω_{sp}, and ω_{ap} modes are highlighted by the corresponding symbols. In the region delimited by a green dot box in (c), the amplitude is multiplied by a factor of 10.

in Fig. 3(c) where the induced density for $q_\parallel = 0.078$ a.u. is presented. At this momentum, one can clearly resolve the enhanced density oscillations across the slab corresponding to both the symmetric mode at $\omega = 8.8$ eV and the antisymmetric one at $\omega = 9.7$ a.u. At this $q_\parallel$, we can also discern the charge density oscillations at $\omega = 0.8$ eV corresponding to a weak acoustic plasmon mode, which still can be found in this slab, however, with very low intensity.

Upon moving to the momentum region where a single surface plasmon mode exists, the corresponding charge density oscillation clearly demonstrates strong localization at the surface exposed to the external perturbation. This is demonstrated in Fig. 3(d) for $q_\parallel = 0.160$ a.u. Here, there is a strong peak in the induced density of conventional monopole character centered at $\omega = 9.6$ eV. It is clearly seen that the maximum of the charge distribution is located outside the surface layer position.

B. *Ab initio* calculations

The main results of present work are shown in Fig. 4 where the surface loss function calculated with full inclusion of the band structure for the 1–5- and 21-ML slabs is displaced. The data presented in this figure correspond to the momentum transfers along the $\overline{\Gamma}$-$\overline{M}$ symmetry direction of the SBZ. We have checked that in the case of Pb films the surface loss functions evaluated at $\mathbf{q}_\parallel$'s along two different high-symmetry directions of the SBZ, namely, $\overline{\Gamma}$-$\overline{M}$ and $\overline{\Gamma}$-$\overline{K}$, are very similar. This isotropic behavior of the surface loss function was found for all the film thicknesses of interest. Thus, from here on, only results for $\mathbf{q}_\parallel$'s along $\overline{\Gamma}$-$\overline{M}$ are shown. Additionally, in Fig. 4, we show by white solid lines the dispersion of the classical hybrid modes $\omega_\pm(q_\parallel)$ given by Eq. (1) using a bulk plasmon energy of 15.5 eV obtained from first-principles calculations [74].

1. *A 21-ML film and Pb(111) surface*

We start the discussion with the surface loss function obtained for a 21-ML slab. This system is also sufficiently thick in order to extract feasible information about the Pb(111) surface excitation spectrum. Comparison of Im$[g(\mathbf{q}_\parallel,\omega)]$ shown in Fig. 4(a) with that for the jellium model of Fig. 2(a)

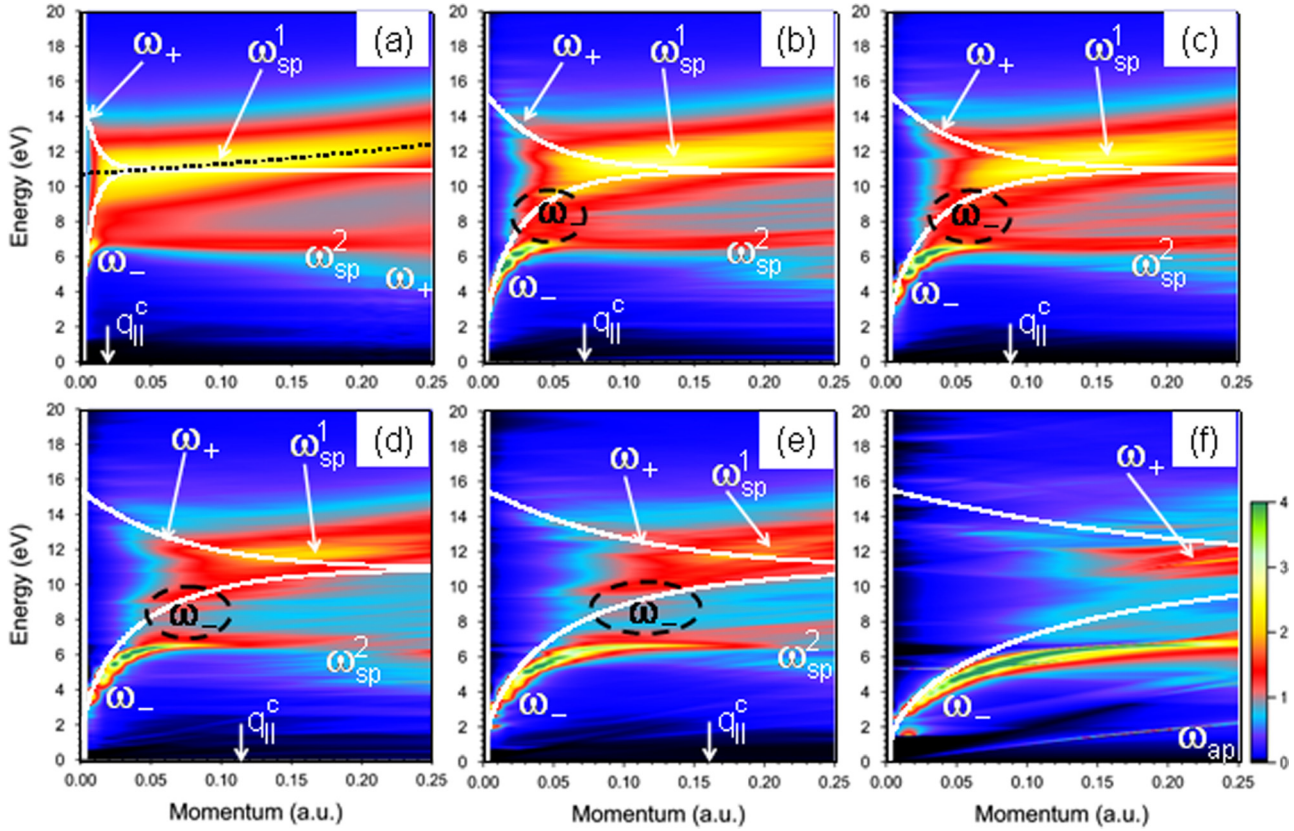

FIG. 4. Surface loss function, Im$[g(\mathbf{q}_\parallel,\omega)]$, for (a) 21-, (b) 5-, (c) 4-, (d) 3-, (e) 2-, and (f) 1-ML-thick Pb(111) slabs calculated with full inclusion of the band structure. The momentum transfer vectors $\mathbf{q}_\parallel$ are directed along $\overline{\Gamma}$-$\overline{M}$. Peaks corresponding to the hybrid slab surface ω_- and ω_+ modes, the ω^1_{sp} and ω^2_{sp} surface plasmons, and acoustic plasmon ω_{ap} are highlighted by the corresponding symbols. In (a), a black dot line shows the interpolated surface plasmon dispersion. Solid white lines present the dispersion of the ω_- and ω_+ hybrid modes according to Eq. (1) with $\omega_p = 15.5$ eV obtained in the first-principles calculation [74]. A position of a critical momentum $q^c_\parallel$ for transition between slab modes and the surface plasmon of a single slab surface is shown as well. A region of transition from a ω_- mode to a ω^1_{sp} mode is denoted by black dash ovals.

reveals that incorporation of the *ab initio* band structure in the density-response calculations strongly modifies the surface excitation spectra of Pb. In Fig. 4(a), one can recognize the following features in the surface loss function obtained in the full first-principles calculation. At finite momentum transfers, one can see two clear peaks in the loss function instead of a single surface plasmon peak of the free-electron model. The upper-energy dominating peak denoted as ω^1_{sp} is located at $\omega \approx 10.8$ eV at small momentum transfers and its energy shifts upward upon momentum increase. From the energy position of this peak and the spatial distribution of the corresponding induced charge density (not shown) we conclude that it corresponds to the surface plasmon of the Pb(111) surface. The calculated energy is in good agreement with the measured value of 10.6 ± 0.2 eV for a surface plasmon [112]. At fairly the same energy, a peak corresponding to the surface plasmon was also observed in recent reflection electron energy loss spectroscopy (REELS) measurements of Pb(111) films absorbed on a Ge substrate [30]. In the available momentum range, the calculated dispersion of the surface plasmon does not present any minimum, in contrast to predictions of the jellium model. It is confirmed by the surface plasmon dispersion deduced from the fitting in Fig. 4(a) of the main ω^1_{sp} peak position at momentum transfers exceeding 0.03 a.u. Its dispersion is described by the equation (expressed in eV)

$$\omega^1_{sp}(q_\parallel) = 10.76 + 4.8 \cdot q_\parallel + 7.8 \cdot q^2_\parallel \qquad (7)$$

and is shown by the black dot line in Fig. 4(a). As evidenced by the positive sign of the linear coefficient in this expression the initial dispersion of the surface plasmon of this surface is positive. Such positive dispersion of the ω^1_{sp} mode is in agreement with experiment [30]. A similar effect of the bulk band structure on the surface plasmon dispersion was observed, for instance, on the silver surfaces [75,113–115].

At lower energies, the calculated spectrum of Fig. 4(a) presents a second peak ω^2_{sp}. The interpolation of its dispersion to small momenta suggests that this peak has an energy of 7.0 eV in the long-wave-length limit. This value is in a close agreement with an additional weak feature measured at 7.2 ± 0.2 eV in the loss spectrum of the Pb surface [112] and at $\approx$7 eV in Pb(111) films [30]. The analysis of spatial distribution of the corresponding charge density suggests that the ω^2_{sp} mode is a result of strong hybridization of the surface plasmon with bulk interband single-particle excitations. This mode originates from the strong modification of the bulk dielectric function in the corresponding energy interval caused by the presence of a broad interband peak IP_2 in the imaginary

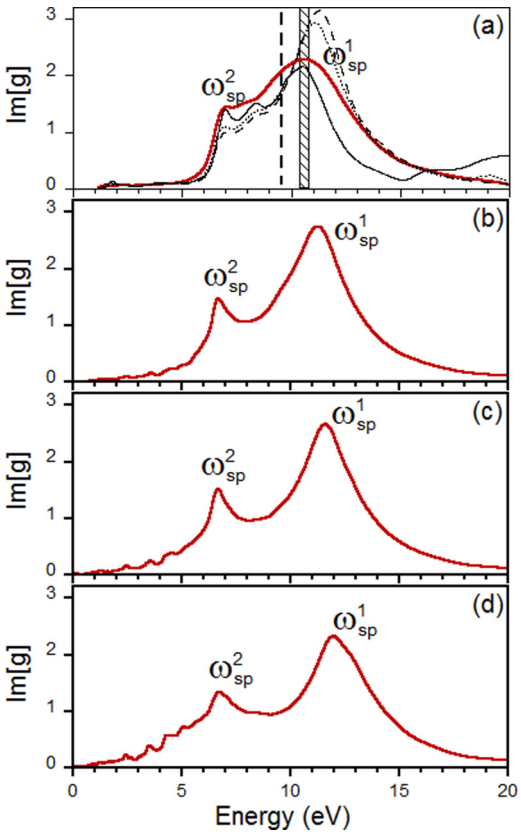

FIG. 5. Red thick solid lines show the loss function of the 21-ML Pb(111) slab at momentum transfers of (a) 0.014, (b) 0.087, (c) 0.142, and (d) 0.206 a.u. along the $\overline{\Gamma}$-$\overline{M}$ direction. Peaks corresponding to the ω^1_{sp} and ω^2_{sp} modes are highlighted by the corresponding symbols. In (a), a thin dash (solid) curve stands for Im[g] deduced from bulk calculations without (with) inclusion of the 5d electrons. The dot line shows the surface loss function deduced from the bulk dielectric function obtained with the spin-orbit coupling included and without 5d states. A vertical dash line in (a) marks a classical Pb surface plasmon energy of 9.57 eV, while the shaded energy interval corresponds to the value of 10.6±0.2 eV measured in the electron energy loss experiment [112].

part of bulk dielectric function, ϵ_2, at energies in the vicinity of 8 eV [30,74]. A similar explanation is given in Ref. [30]. An interesting feature of this mode is its almost flat dispersion over the entire momentum range being, again, in agreement with the experiment. Because of such a dispersion, the energy separation of the ω^2_{sp} mode from the upper ω^1_{sp} one increases upon momentum increase resulting in a better definition of this mode. This can be seen in Fig. 5 where the surface loss function for a 21-ML film at four momentum transfers is reported. In Fig. 5(a), in the loss spectrum corresponding to $q_\parallel = 0.014$ a.u., one can see that it is dominated by a broad peak with an energy of ∼10.8 eV, whereas the second peak at ∼7 eV is less defined. However, upon momentum increase and gradual energy separation between both these peaks, the ω^2_{sp} peak becomes more clearly defined as evidenced from the loss spectra at $q_\parallel = 0.087$, 0.142, and 0.206 a.u. reported in Figs. 5(b)–5(d), respectively.

It is interesting to compare the calculated surface plasmon energies with the classical results. In Fig. 5(a), the vertical dash line marks the classical surface plasmon energy $\omega_s = \omega_p/\sqrt{2} = \sqrt{1.5 r_s^{-3}}$, which for the averaged valence electron density of bulk lead $r_s^{Pb} = 2.298$ gives the value $\omega_s^{Pb} = 9.57$ eV. Also, the results of the experimental electron energy-loss measurements [112] of 10.6 ± 0.2 eV are represented by the thin shaded area. As can be seen, the classical expression gives a too low value of the surface plasmon energy by about 1 eV.

The surface loss function of 21-ML Pb(111) slab calculated at small momentum transfers can be contrasted with the data obtained from the bulk dielectric function since in the optical limit ($q_\parallel \to 0$) the surface response function is determined by the bulk dielectric function $\varepsilon^{bulk}(q_\parallel \to 0,\omega)$ as [32,93]

$$g(q_\parallel \to 0,\omega) = \frac{\varepsilon^{bulk}(q_\parallel \to 0,\omega) - 1}{\varepsilon^{bulk}(q_\parallel \to 0,\omega) + 1}. \quad (8)$$

In Fig. 5(a), a thin dash (solid) curve represents Im[$g(q_\parallel \to 0,\omega)$] calculated according to Eq. (8) with the inclusion of the 5d electrons in the core (valence) shell in the calculation of the bulk dielectric function. In agreement with the explicit calculation for the 21-ML Pb(111) slab, the shape of these curves can not be described by a single peak. The energy of the dominating peak is of 11.2 (10.5) eV with the semicore 5d electrons excluded from (included in) the valence configuration. The surface plasmon energy evaluated using the bulk dielectric function obtained with the 5d electrons included is close to the experimental one of 10.6 ± 0.2 eV [112]. Also the positions of peaks in Im[$g(q_\parallel \to 0,\omega)$] calculated from the knowledge of $\varepsilon^{bulk}(q_\parallel \to 0,\omega)$ obtained with inclusion of the 5d electrons is closer to the loss function calculated explicitly at small momentum transfer [a red thick solid line in Fig. 5(a)]. It is interesting to note that Im[$g(q_\parallel \to 0,\omega)$] in both curves obtained on the basis of the bulk dielectric function also have a peak at 6.9 eV, confirming in such a way the origin of the ω^2_{sp} mode in the bulk electronic structure.

As is mentioned above, the present calculations of the surface loss function were performed at the scalar-relativistic level without taking explicitly into account the spin-orbit interaction. Nevertheless, one can estimate its impact on the surface excitation spectrum by employing the bulk dielectric function obtained with spin-orbit interaction included in the evaluation of Im[$g(q_\parallel \to 0,\omega)$]. The corresponding data are presented in Fig. 5(a) by a thin dot line. From its comparison with the dash line, one may deduce that the spin-orbit interaction may introduce visible modifications in the evaluated surface loss function. However, these modifications are mainly related to the shape of the loss spectrum, with a possible shift of the peak energies not exceeding 0.2 eV. However, as it is clear from comparison of thin dash and solid lines in Fig. 5(a), inclusion of the 5d electrons would have a much stronger effect on the loss spectrum. In this situation, we consider that incorporation of the spin-orbit interaction in the calculation of the surface loss function of Pb is not justified due to an enormous calculation cost it implies.

Upon close inspection of Figs. 4(a) and 5(a), a weak peak can be discerned in the low-energy side of the spectrum. Its presence correlates with the REELS measurements of Ref. [30] where a third notable feature at small momentum transfers is observed at energies in the vicinity of 1.5 eV.

However, although in the calculated surface loss function of Fig. 5(a) a peak is also present at $\omega \sim 1.5$ eV, its strength is significantly reduced in comparison with the other two peaks corresponding to the ω^1_{sp} and ω^2_{sp} modes. One of the reasons why in the experiment the intensity of the 1.5 eV peak is comparable with that of the other two modes could reside in the dependence of the excitation probability of all these modes on the experimental conditions. On the other hand, the Ge substrate used in the experiment of Ref. [30] might play some role as well.

2. *Ultrathin Pb(111) films*

Reduction of the film thickness allows us to investigate in detail the transformation of the surface plasmons linked to each slab surface into the fundamental ω_- and ω_+ hybrid modes and its interaction with the bulk single-particle excitations. Thus, in the surface loss function of the 5-ML Pb(111) film of Figs. 4(b) and 6 at momentum transfers exceeding the critical value $q^c_\parallel = 0.07$ a.u., two peaks corresponding to the surface plasmons

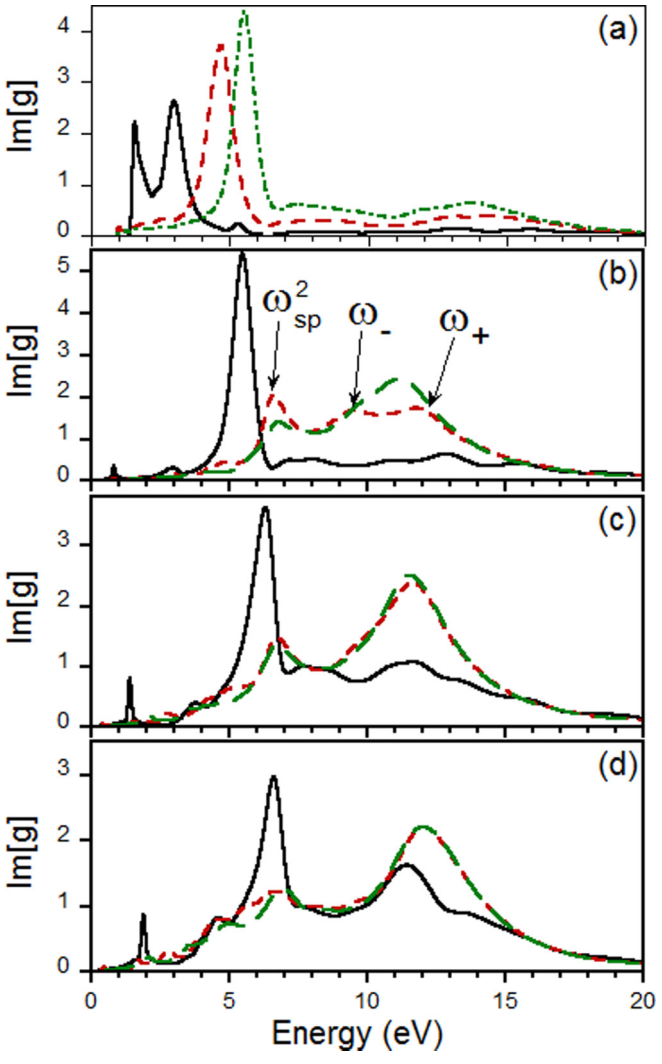

FIG. 6. Surface loss function for different film thicknesses at $q_\parallel$ of (a) 0.014, (b) 0.087, and (c) 0.142, and (d) 0.206 a.u. Black solid, red dash, and green dash-dot curves represent results for 1-, 3-, and 5-ML films, respectively.

found in the thick 21-ML film can be seen. It correlates with the REELS experiment where the 7 and 10 eV features persist in the Pb films with thicknesses down to 5 ML [30]. As in the 21-ML slab, at larger momentum transfers, the upper-energy ω^1_{sp} mode disperses upward with momentum increase, whereas the lower-energy one is almost dispersionless. Additionally, numerous weak peaks with significantly lower intensities can be found in the surface loss function in the same energy interval due to quantization of the electronic states.

However, expansion of the momentum transfer region where two hybrid plasmon modes coexist allows us to observe an interesting effect. Thus, in Fig. 4(b), at $q_\parallel$'s close to a value of 0.05 a.u., instead of two conventional slab plasmon peaks, one can detect three peaks. At $q_\parallel$'s close to this value, the lower-energy ω_- mode splits into two peaks: a sharp lower energy peak evolving into a dispersionless ω^2_{sp} eV mode and a broad peak in the 7–10 eV region highlighted by a black dash oval in Fig. 4(b). The latter peak dispersion actually represents qualitatively the symmetric ω_- mode dispersion, as can be concluded from comparison with the dispersion of the corresponding solid white line of a classical model in Fig. 4(b).

Qualitatively, the same picture is observed in the surface loss function of the 4- and 3-ML Pb(111) films presented in Figs. 4(c) and 4(d), respectively. Again, at momentum transfers exceeding $q^c_\parallel$, which in turn gradually shifts to higher values upon the thickness reduction, two clear ω^1_{sp} and ω^2_{sp} peaks are seen. In the intermediate momentum region, the three ω^2_{sp}, ω_-, and ω_+ peaks are realized as well. Even in the 2-ML film, a signature of the ω_- mode in the 7–10 eV energy interval can be seen in the surface loss function as highlighted by the black dash oval in Fig. 4(e). This fact allows us to interpret the upper-energy peak at $q_\parallel$'s exceeding a critical $q^c_\parallel \sim 0.16$ a.u. as a surface plasmon mode.

In the 2-ML film, at lower momentum transfers, the upper energy antisymmetric ω_+ exists as a well-defined collective excitation at momenta exceeding 0.08 a.u., whereas the lower-energy symmetric ω_- mode is well defined up to $q_\parallel \sim 0.16$ a.u. Figure 4(e) reveals that at larger momentum transfers the corresponding peak in the surface loss function starts to experience a strong hybridization with the one-particle transitions. Similar hybridization of this mode can be noted at momenta smaller than 0.015 a.u. where there exists a threshold at energy of ~1 eV for the intense bulklike interband transitions [73] resulting in a ω^2_{sp} mode at larger momenta. This interaction is even stronger in the 1-ML film resulting in the splitting of the ω_- plasmon peak in two peaks as seen in Fig. 4(f). In more detail it is seen in the surface loss function of the 1-ML film at $q_\parallel = 0.014$ a.u. of Fig. 6(a), where in the black solid curve instead of a single peak corresponding to a ω_- mode, two sharp peaks at 1.5 and 3 eV are present. In the loss function of the 1-ML film, a peak in the 7–10 eV energy interval is not observed. Instead, two never merged plasmon modes ω_- and ω_+ are realized.

In Figs. 4(b)–4(f), one can observe the dispersion of the hybrid ω_- mode over an extraordinary broad energy interval ranging from ~7 eV down to zero. This energy interval largely exceeds that exploited in the noble metal and graphene plasmonics [116–118]. From the calculated dispersion, one can deduce that a similar in-plane spatial confinement may be

achieved in the thin Pb films. Moreover, by changing the film thickness, the ω_- mode dispersion can be varied in a broad range.

Close inspection of Fig. 4(f) confirms the presence of a well-defined peak with a sound-like dispersion in the low-energy part of the spectrum. The corresponding peak, denoted as ω_{ap}, can be well resolved over the entire momentum range starting from zero energy in the $q \to 0$ limit and reaching an energy of 2.3 eV at $q_\parallel = 0.25$ a.u. As in a jellium model case, we trace the appearance of this mode to the presence of several energy bands crossing the Fermi level with different Fermi velocities as seen in Fig. 1(a). As a result, the dynamical screening of the slow carriers in one band by the fast carriers in the other leads to the realization of a mode with a such a dispersion. From Figs. 4(f) and 6(d), it is seen that at finite momentum transfers the corresponding peak in the loss function of the 1-ML film has significant intensity in comparison with other modes.

In the calculation for a free-standing 1-ML slab, the acoustic surface plasmon has a group velocity of 9.2 eV·a.u. This value can be compared with the group velocity of a 2D acoustic plasmon (21.8) eV·a.u. measured in a Pb/Si(557) surface at a Pb coverage close to the 1 ML [29]. The linear dispersion of this mode measured in the loss experiment confirms that at this surface at least two energy bands cross the Fermi level. At the same time, the measured group velocity signals that the Fermi velocity in the band with lower carriers is about two times larger than that obtained for a free-standing Pb monolayer. On the other hand, a $\sqrt{q_\parallel}$-like dispersion of the 2D plasmon also found in Ref. [29] for almost the same coverage of Pb on Si(111) may signal the presence of one or more energy bands crossing the Fermi level with similar Fermi velocities. In the surface loss function of thicker films of Figs. 4(b)–4(e), one can discern in the low-energy interval some peaks with similar dispersion. However, its intensity is extremely low and it is difficult to prove its collective nature.

As is discussed above, the calculations of the surface excitation spectra include several ingredients. Some of them, like the slab band structure and local-field effects in the direction perpendicular to the surface, are explicitly taken into account in the current calculations. A possible effect of other ingredients, like semicore $5d$ electrons and spin-orbit interaction, is discussed above on the basis of the bulk dielectric function. Here, we intend to demonstrate what effect may the inclusion of the in-plane local-field effects have on the calculated spectrum, i.e., fully taking into account the 3D nature of the surface response function. For this, we performed calculations of Im$[g(\mathbf{q}_\parallel,\omega)]$ of the 3-ML slab employing full 3D $\mathbf{G}$ vectors in the expression (5) for $\chi^0_{\mathbf{G}\mathbf{G}'}$. Such calculated χ^o was employed in the evaluation of χ according to Eq. (4) followed by its use in Eq. (2). In Fig. 7, we compare Im$[g]$ calculated for three values of $q_\parallel$ with the use of 1D and 3D representations for the $\mathbf{G}$ vectors. It is clearly seen that at small $q_\parallel$, Fig. 7(a), the resulting curves are almost identical. Only in the 6–10 eV energy interval some difference can be detected, whereas the peaks corresponding to the hybrid ω_- and ω_+ modes are insensitive to the in-plane local fields. Upon momentum increase, the deviation between curves of two models becomes to be more notable. Thus the intensity of three peaks ω^2_{sp}, ω_-, and ω_+ at $q_\parallel = 0.096$ a.u. in Fig. 7(b) changes notably upon taking the full 3D screening

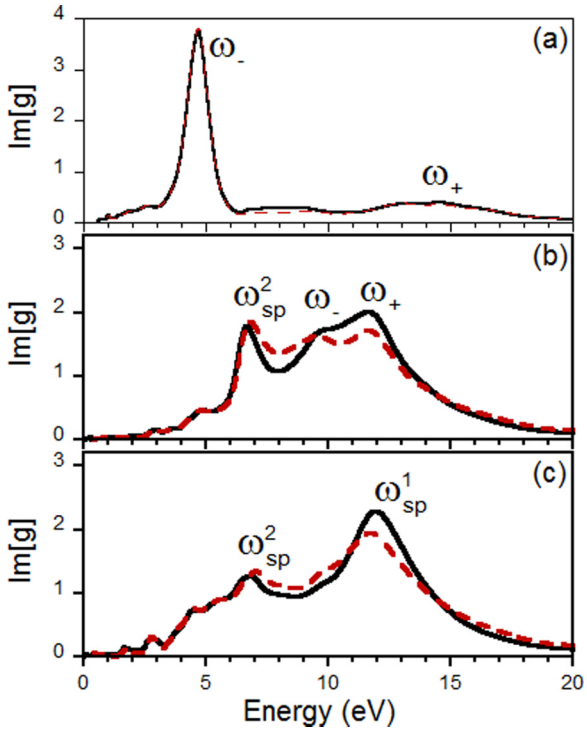

FIG. 7. Surface loss function of the 3-ML slab calculated at $q_\parallel$ of (a) 0.014, (b) 0.096, and (c) 0.192 a.u. Solid (dash) lines show results obtained without (with) inclusion of the in-plane local field effects. Peaks related to the different modes are denoted by the corresponding symbols.

into account. Nevertheless, the energy position of these peaks is maintained almost intact. When the momentum increases up to 0.192 a.u., some changes in the energy position of the peaks in the calculated surface loss function become more visible. As seen in Fig. 7(c), the incorporation of the in-plane local fields produces the downward shift of the ω^1_{sp} peak by ≈0.2 eV and upward shift of the ω^2_{sp} one by ≈0.3 eV. It is accompanied by a modification in the intensities of these two peaks as well, i.e., the intensity of the ω^1_{sp} peak reduces and that of the ω^2_{sp} mode increases. We expect that the same trend should be realized for the films of other thicknesses and the Pb(111) surface as well. This analysis demonstrates that a possible impact of inclusion of the in-plane local fields on the surface loss spectrum is on the same level as the spin-orbit interaction. Taking into account that upon transition from 1D to 3D representation for the $\mathbf{G}$ vectors in the χ^o expansion the number of the vectors increases in the case of the 3-ML slab by a factor of 25 accompanied by an increase in the computation cost in the same scale, we conclude that a possible improvement in the calculated spectra does not justify the use of a 3D $\mathbf{G}$ representation in the evaluation of g for this material.

In order to illustrate the spatial localization of collective excitations of the slabs, in Fig. 8, the imaginary part of the 2D Fourier transform of the induced density, Im$[n^{ind}(z,\mathbf{q}_\parallel,\omega)]$, is shown as a function of energy and distance z for the 4-ML slab. The results correspond to four values of momentum transfer $q_\parallel$, thus demonstrating different regimes. At a small momentum, Fig. 8(a), it is easy to detect the oscillating charge corresponding to the symmetric ω_- and antisymmetric ω_+

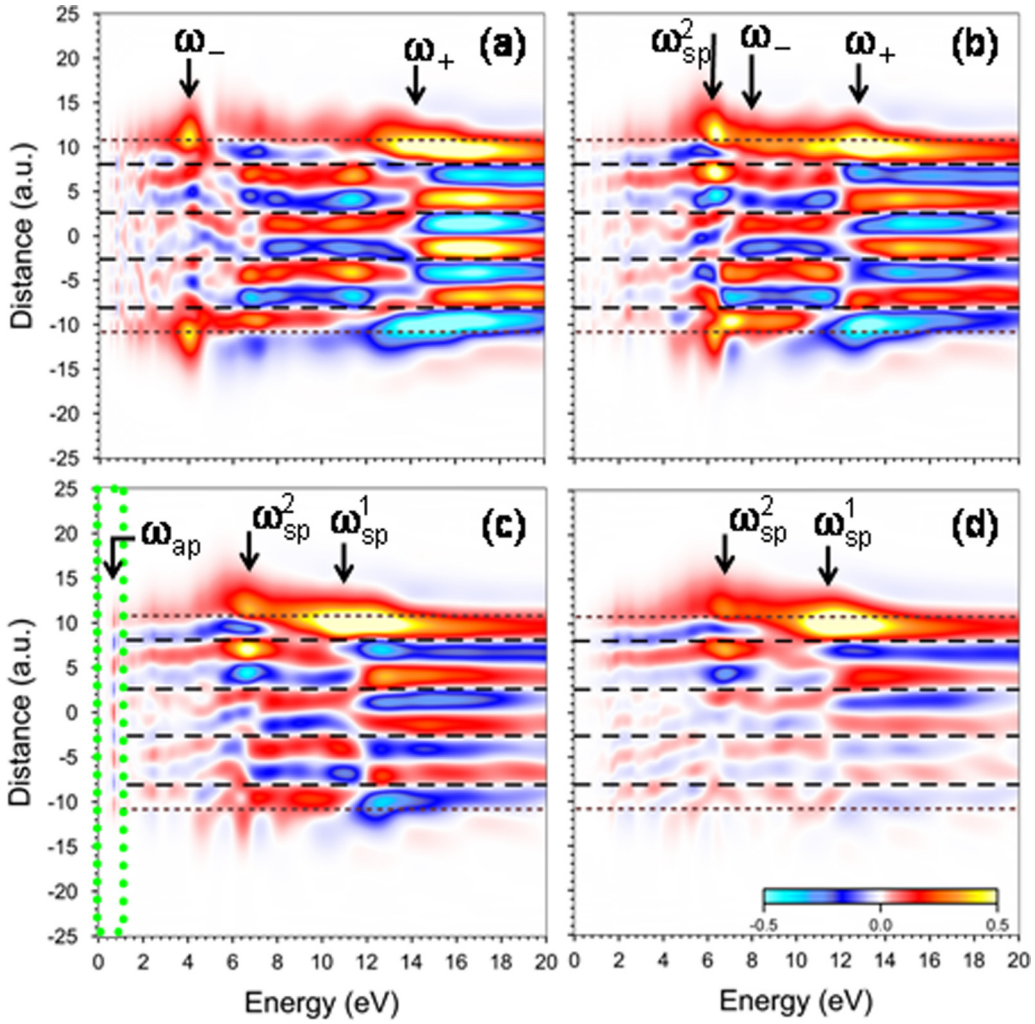

FIG. 8. Imaginary part of the induced density for the 4-ML Pb(111) film at $q_\parallel$= (a) 0.009, (b) 0.041, (c) 0.078, and (d) 0.160 a.u., as a function of the energy transfer ω and the z coordinate. Calculations are performed with full inclusion of the slab band structure. Horizontal dot and dash lines mark the slab edges and the atomic layer positions. Charge oscillations corresponding to the ω_-, ω_+, ω^1_{sp}, ω^2_{sp}, and ω_{ap} are highlighted by the corresponding symbols. In the region delimited by a green dot box in (c), the amplitude is multiplied by a factor of 5.

modes. In the former case, the charge has a clear symmetric distribution with respect to the center of slab, whereas in the latter case the charge distribution is antisymmetric. In the density distribution at $q_\parallel = 0.041$ a.u. of Fig. 8(b), the situation is more complex. At this momentum, two dominating oscillations still present with essentially symmetric (corresponding to a ω^2_{sp} mode) and antisymmetric (a ω_+ mode) distributions. However, in the former case, the charge distribution is strongly affected by interaction with bulklike single-particle transitions and significant deviation from the symmetric distribution is evident. In this figure, one can also detect the oscillating charge corresponding to the slab ω_- mode. However, these oscillations strongly broaden in energy in accordance with the strong broadening of the corresponding peak in the loss function of Fig. 4(c).

At $q_\parallel = 0.078$ a.u., charge oscillations related to the ω^1_{sp} and ω^2_{sp} surface modes can be seen in Fig. 8(c). It is interesting to compare the corresponding $\mathrm{Im}[n^{\mathrm{ind}}]$ with the jellium model result reported in Fig. 3(c). At this $q_\parallel$ in the jellium model, two slab modes are still observed with maxima of induced density located close to the film surface layer, below the crystal edge. However, in the case of Fig. 8(c), the maximum of charge distribution of the ω^2_{sp} mode is located outside the crystal edge. Also strong charge oscillations are observed at these energies over the whole slab. Additionally, in the low-energy region highlighted in Fig. 8(c) by green dot box the charge oscillations attributed to the ω_{ap} mode can be resolved as well.

Once momentum reaches $q_\parallel = 0.160$ a.u., the formation of the ω^1_{sp} and ω^2_{sp} modes is completed as evidenced from Fig. 8(d). The spatial localization of the charge corresponding to both these modes occurs in the out-of-phase fashion. The distribution corresponding to the ω^2_{sp} mode is extended into the vacuum side in comparison with that corresponding to the ω^1_{sp} mode. The positive charge of ω^1_{sp} mode is located at z's where essentially negative $\mathrm{Im}[n^{\mathrm{ind}}]$ of the ω^2_{sp} one is realized.

Comparison of charge distribution in Figs. 3 and 8 reveals that, according to the jellium model, in the upper energy interval of Fig. 3, the amplitude of the charge oscillations is negligible. In contrast, in Fig. 8, the amplitude of such charge oscillations obtained in the first-principles calculations

is comparable with that corresponding to the surface plasmon. Such behavior is explained by a strong broadening of the surface plasmon ω^1_{sp} peak due to decay into single-particle excitations.

3. *Lifetime*

From the calculated surface loss function of the 21-ML Pb(111) film presented in Figs. 4 and 5 one can obtain, besides the energy dispersion, another important characteristic of the surface plasmon modes, its lifetime, which is inversely proportional to the peak width. In Fig. 5(a), the linewidth of the dominating ω^1_{sp} peak exceeds 2 eV, i.e., its lifetime is shorter than 0.3 fs. The extracted linewidth of the ω^2_{sp} mode is around 0.4 eV, i.e., its lifetime is around 1.5 fs. Such values for lifetime are significantly shorter than those characteristics of noble metals. It seems, this excludes lead as a material interesting for plasmonic applications. However, in the surface loss function of Fig. 4(a), one can observe how at small $q_\parallel$'s the ω^2_{sp} peak width quickly narrows upon transformation into the ω_- hybrid mode following the same scenario as in the jellium model of Fig. 2(a). In a similar fashion, when the momentum transfer becomes smaller than a critical momentum $q^c_\parallel$, in the surface loss function of Fig. 4(a) two separate hybrid symmetric ω_- and antisymmetric ω_+ modes emerge. In the case of the upper-energy ω_+ mode, its dispersion follows rather closely the curve described by Eq. (1) of the classical model. On contrary, in the full calculation, the dispersion of the ω_- mode is strongly affected by the band structure. In particular, its dispersion goes at a notably lower energy in comparison with that of the dispersion curve predicted by a classical model. Unfortunately, due to the finite resolution in $q_\parallel$, we can not investigate in detail this small-$q_\parallel$ region in the case of the 21-ML slab. However, it can be done studying the thinner slabs as demonstrated below.

In Fig. 9(a), we collect the extracted linewidth Γ_- of the ω_- peak obtained in the full calculations for the 1–5-ML slabs versus its energy. These data show how the linewidth of this mode strongly depends on the slab thickness. Thus, in the 3–4 eV energy interval, its value can vary from $\approx$1 eV for 5-ML slab to less than 0.4 eV in the 2-ML case. Another observation consists in a strong variation of the linewidth of a given slab with excitation energy. Moreover, for some slabs, e.g., the 2-ML slab, these variations present a clear oscillatory behavior. A possible explanation for the oscillating behavior of Γ_- is in the quantization of energy bands seen in Fig. 1. As a result, the energy separation between the occupied and unoccupied energy bands is different for slabs of different thicknesses.

One of the curious trends in the data of Fig. 9(a) is that the linewidth in general reduces with the energy increase in the 3–7 eV energy interval. This is in stark contrast with the jellium model results reported for comparison in Fig. 9(b). In order to explain such behavior, one should refer to the bulk dielectric function of lead [30,74]. In particular, one can see a strong interband peak at $\sim$2.5 eV in the imaginary part of bulk dielectric function, ϵ_2, accompanied by a shallow minimum at $\sim$6.5 eV. As a result, ϵ_2 slowly decays with the energy increase in the 2.5–6.5 eV energy interval. The corresponding reduction of the scattering probability into the single-particle excitations is reflected in the plasmon linewidth.

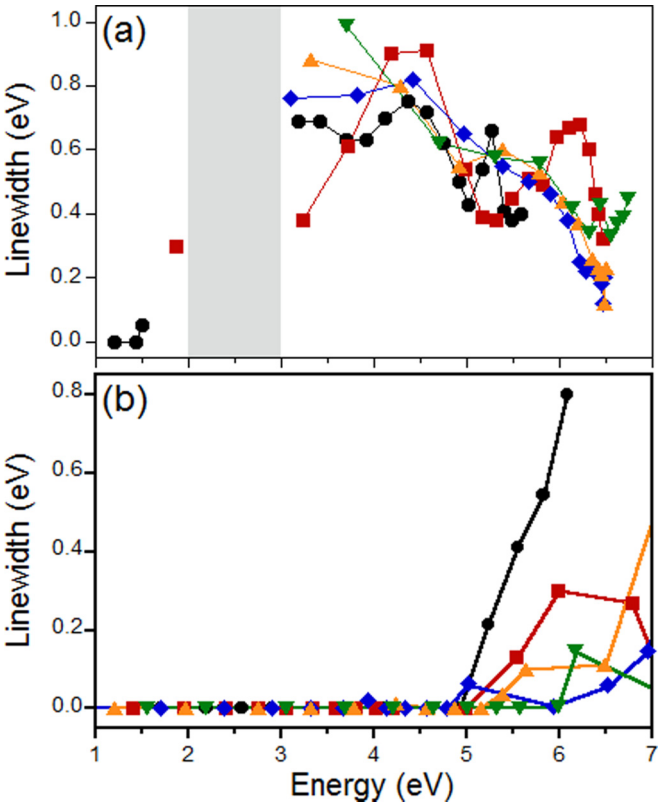

FIG. 9. Linewidth vs energy of the hybrid ω_- mode in (a) *ab initio* and (b) jellium models for 1- (circles), 2- (squares), 3- (diamonds), 4- (triangles), and 5- (inverted triangles) ML slabs. Gray region shows the energy interval, where strong interaction with the interband single-particle transition prevents the formation of such a mode.

Additionally, in Fig. 9(a), one can detect the 2–3 eV energy interval where the ω_- mode is not realized due to strong hybridization with the bulklike interband single-particle excitations. Again, it is related to the presence at those energies of the above-mention peak in bulk ϵ_2. Curiously, this gap appears even in the 1-ML film, which reflects the fact that screening in Pb occurs at distances comparable with the atomic interlayer distance. The presence of such a gap in the plasmon dispersion was observed in the REELS experiment [30] as well.

From Fig. 9(a), one can deduce that a minimum in the linewidth Γ_- of the ω_- mode can be reached at energies below 2 eV. The Γ_- values obtained for this interval suggest that the intrinsic lifetime of this mode in Pb films can be comparable to that of noble metals. At larger energies, the minima in Γ_- can be expected at energies around 5 and 6.5 eV.

V. CONCLUSIONS

The present first-principles study shows strong effects of full inclusion of the electronic band structure on the excitation spectrum of the Pb(111) free-standing films of different thicknesses. In the case of thin films consisting of a few atomic layers, the calculated surface loss function allows for investigation of transformation of a low-energy symmetric hybrid mode found at small momentum transfers into two surface modes upon momentum increase. The details

of formation of the upper-energy antisymmetric hybrid mode in such thin films are also presented. Additionally, in the 1-ML Pb(111) film, we find a well defined peak corresponding to the acoustic plasmon mode. Its existence correlates with the 2D plasmon with a soundlike dispersion measured on the 1-ML Pb/Si(557) surface [29].

Investigation of the surface loss function of a thick Pb(111) slab consisting of 21 MLs allows us to obtain information about the loss excitation spectrum of the corresponding surface. The main effect of the realistic band structure on the surface loss function is a splitting of the surface plasmon into two surface modes. The dominating surface mode has energy of 10.76 eV at small momenta and has positive dispersion at all momentum transfers studied. Such value is in a good agreement with the surface plasmon energy of 10.6 ± 0.2 eV obtained in the electron loss experiment [112]. The lower-energy surface mode has energy of $\sim$7 eV and is almost dispersionless. The optical surface loss function evaluated from bulk calculations also shows a faint peak at $\sim$7 eV. Identification of this mode in our calculation is in agreement with the presence of a peak at energy of 7.2 ± 0.2 eV in the surface loss spectrum measured in the same experiment [112]. The linewidth analysis of the surface mode peaks shows that the lifetime of such excitations in Pb thin films may depend strongly on the number of monolayers in a film and the excitation energy due to the interband bulklike excitations in certain energy intervals.

Additionally, we have estimated a possible impact of several factors on the excitation spectra of the Pb thin films and its surface. In particular, we have shown that taking into account spin-orbit interaction may change the energy of the fundamental modes within 0.2 eV. We have also estimated a possible impact of a full inclusion of the in-plane local-field effects on plasmon energies in case of a 3-ML Pb(111) and found that the respective energy change does not exceed 0.3 eV. Evaluation of the surface loss function for a Pb surface based on the bulk dielectric function suggests that the semicore 5*d* electronic states may affect the energy of collective excitations in the considered systems more notably. To quantify this effect, explicit calculations of surface loss function are needed. We believe that new electron energy loss spectroscopy measurements on a Pb clean surface and a few-ML thin films are highly desirable to check the present predictions and gain further insight in the dynamics of collective excitations of nanostructured systems.

ACKNOWLEDGMENTS

E.V.C. and V.M.S. acknowledge the partial support from the University of the Basque Country UPV/EHU, Grant No. IT-756-13, and the Spanish Ministry of Economy and Competitiveness MINECO, Grant No. FIS2016-76617-P.

[1] T.-C. Chiang, Surf. Sci. Rep. **39**, 181 (2000).
[2] B. J. Hinch, C. Koziol, J. P. Toennies, and G. Zhang, Europhys. Lett. **10**, 341 (1989).
[3] M. M. Ozer, J. R. Thompson, and H. H. Weitering, Nat. Phys. **2**, 173 (2006).
[4] I. Y. Sklyadneva, G. Benedek, E. V. Chulkov, P. M. Echenique, R. Heid, K.-P. Bohnen, and J. P. Toennies, Phys. Rev. Lett. **107**, 095502 (2011).
[5] R. Díez Muiño, D. Sańchez-Portal, V. M. Silkin, E. V. Chulkov, and P. M. Echenique, Proc. Natl. Acad. Sci. U. S. A. **108**, 971 (2011).
[6] I. Y. Sklyadneva, R. Heid, K.-P. Bohnen, P. M. Echenique, and E. V. Chulkov, Phys. Rev. B **87**, 085440 (2013).
[7] Y. Jia, B. Wu, H. H. Weitering, and Z. Y. Zhang, Phys. Rev. B **74**, 035433 (2006).
[8] R. Otero, A. L. Vazquez de Parga, and R. Miranda, Phys. Rev. B **66**, 115401 (2002).
[9] F. Yndurain and M. P. Jigato, Phys. Rev. Lett. **100**, 205501 (2008).
[10] J. Braun, P. Ruggerone, G. Zhang, J. P. Toennies, and G. Benedek, Phys. Rev. B **79**, 205423 (2009).
[11] M. Jalochowski, M. Hoffmann, and E. Bauer, Phys. Rev. Lett. **76**, 4227 (1996).
[12] P. S. Kirchmann, M. Wolf, J. H. Dil, K. Horn, and U. Bovensiepen, Phys. Rev. B **76**, 075406 (2007).
[13] J. Kim, S. Qin, W. Yao, Q. Niu, M. Y. Chou, and C.-K. Shih, Proc. Natl. Acad. Sci. USA **107**, 12761 (2010).
[14] I.-P. Hong, C. Brun, F. Patthey, I. Y. Sklyadneva, X. Zubizarreta, R. Heid, V. M. Silkin, P. M. Echenique, K. P. Bohnen, E. V. Chulkov, and W.-D. Schneider, Phys. Rev. B **80**, 081409(R) (2009).
[15] P. S. Kirchmann, L. Rettig, X. Zubizarreta, V. M. Silkin, E. V. Chulkov, and U. Bovensiepen, Nat. Phys. **6**, 782 (2010).
[16] A. Politano and G. Chiarello, Prog. Surf. Sci. **90**, 144 (2015).
[17] T. Zhang, P. Cheng, W.-J. Li, Y.-J. Sun, G. Wang, X.-G. Zhu, K. He, L. Wang, X. Ma, X. Chen, Y. Wang, Y. Liu, H.-Q. Lin, J.-F. Jia, and Q.-K. Xue, Nat. Phys. **6**, 104 (2010).
[18] C. Brun, I.-P. Hong, F. Patthey, I. Y. Sklyadneva, R. Heid, P. M. Echenique, K. P. Bohnen, E. V. Chulkov, and W.-D. Schneider, Phys. Rev. Lett. **102**, 207002 (2009).
[19] C. Tegenkamp, Z. Kallassy, H. Pfnür, H.-L. Günter, V. Zielasek, and M. Henzler, Phys. Rev. Lett. **95**, 176804 (2005).
[20] C. Tegenkamp and H. Pfnür, Surf. Sci. **601**, 2641 (2007).
[21] C. Tegenkamp, T. Ohta, J. L. McChesney, H. Dil, E. Rotenberg, H. Pfnür, and K. Horn, Phys. Rev. Lett. **100**, 076802 (2008).
[22] C. Tegenkamp, D. Lükermann, S. Akbari, M. Czubanowski, A. Schuster, and H. Pfnür, Phys. Rev. B **82**, 205413 (2010).
[23] M. Czubanowski, A. Schuster, H. Pfnür, and C. Tegenkamp, Phys. Rev. B **77**, 174108 (2008).
[24] J.-F. Jia, S.-C. Li, Y.-F. Zhang, and Q.-K. Xue, J. Phys. Soc. Jpn. **76**, 082001 (2007).
[25] M. Özer, C. Wang, Z. Zhang, and H. H. Weitering, J. Low Temp. Phys. **157**, 221 (2009).
[26] M. Jałochowski, M. Strożak, and R. Zdyb, Phys. Rev. B **66**, 205417 (2002).
[27] M. Jałochowski, M. Strożak, and R. Zdyb, J. Phys.: Condens. Matter **16**, S4345 (2004).

[28] A. Pucci, F. Kost, G. Fahsold, and M. Jalochowski, Phys. Rev. B **74**, 125428 (2006).
[29] H. Pfnür, C. Brand, M. Jäger, J. P. Rönspies, and C. Tegenkamp, Surf. Sci. **643**, 79 (2016).
[30] A. Teng, Ph.D thesis, University of Tennessee, Knoxville, 2014.
[31] R. H. Ritchie, Phys. Rev. **106**, 874 (1957).
[32] A. Liebsch, *Electronic Excitations at Metal Surfaces* (Plenum, New York, 1997).
[33] J. M. Pitarke, V. M. Silkin, E. V. Chulkov, and P. M. Echenique, Rep. Prog. Phys. **70**, 1 (2007).
[34] Z. Yuan and S. Gao, Phys. Rev. B **73**, 155411 (2006).
[35] F. Stern, Phys. Rev. Lett. **18**, 546 (1967).
[36] V. M. Silkin, E. V. Chulkov, and P. M. Echenique, Phys. Rev. Lett. **93**, 176801 (2004).
[37] V. M. Silkin and E. V. Chulkov, Vacuum **81**, 186 (2006).
[38] V. M. Silkin, E. V. Chulkov, and P. M. Echenique, Radiat. Eff. Defects Solids **162**, 483 (2007).
[39] J. Yan, J. J. Mortensen, K. W. Jacobsen, and K. S. Thygesen, Phys. Rev. B **83**, 245122 (2011).
[40] J. Yan, K. W. Jacobsen, and K. S. Thygesen, Phys. Rev. B **84**, 235430 (2011).
[41] J. Yan, K. W. Jacobsen, and K. S. Thygesen, Phys. Rev. B **86**, 241404(R) (2012).
[42] W. Ming, S. Blair, and F. Liu, J. Phys.: Condens. Matter **26**, 505302 (2014).
[43] N. Tancogne-Dejean, C. Giorgetti, and V. Veniard, Phys. Rev. B **92**, 245308 (2015).
[44] A. J. Bennett, Phys. Rev. B **1**, 203 (1970).
[45] C. Schwartz and W. L. Schaich, Phys. Rev. B **26**, 7008 (1982).
[46] N. D. Lang and W. Kohn, Phys. Rev. B **1**, 4555 (1970).
[47] A. G. Eguiluz, Phys. Rev. Lett. **51**, 1907 (1983).
[48] A. G. Eguiluz, Phys. Rev. B **31**, 3303 (1985).
[49] J. A. Gaspar, A. G. Eguiluz, K.-D. Tsuei, and E. W. Plummer, Phys. Rev. Lett. **67**, 2854 (1991).
[50] J. F. Dobson, Phys. Rev. B **46**, 10163 (1992).
[51] W. L. Schaich and J. F. Dobson, Phys. Rev. B **49**, 14700 (1994).
[52] A. Liebsch, B.-O. Kim, and E. W. Plummer, Phys. Rev. B **63**, 125416 (2001).
[53] Y. Yu, Y. Jiang, Z. Tang, Q. Guo, J. Jia, Q. Xue, K. Wu, and E. Wang, Phys. Rev. B **72**, 205405 (2005).
[54] Y. Yu, Z. Tang, Y. Jiang, K. Wu, and E. Wang, Surf. Sci. **600**, 4966 (2006).
[55] Z. Yuan and S. Gao, Surf. Sci. **602**, 460 (2008).
[56] Z. Yuan, Y. Jiang, Y. Gao, M. Käll, and S. Gao, Phys. Rev. B **83**, 165452 (2011).
[57] X. Li, A. Teng, M. M. Özer, J. Shen, H. H. Weitering, and Z. Zhang, New. J. Phys. **16**, 065014 (2014).
[58] Z. Yuan and S. Gao, Comp. Phys. Commun. **180**, 466 (2009).
[59] L. Marušić, V. Despoja, and M. Šunjić, J. Phys.: Condens. Matter **18**, 4253 (2006).
[60] A. Politano, V. M. Silkin, I. A. Nechaev, M. S. Vitiello, L. Viti, Z. S. Aliev, M. B. Babanly, G. Chiarello, P. M. Echenique, and E. V. Chulkov, Phys. Rev. Lett. **115**, 216802 (2015).
[61] J. Zuloaga, E. Prodan, and P. Nordlander, Nano Lett. **9**, 887 (2009).
[62] P. Song, P. Nordlander, and S. Gao, J. Chem. Phys. **134**, 074701 (2011).
[63] D. C. Marinica, A. K. Kazansky, P. Nordlander, J. Aizpurua, and A. G. Borisov, Nano Lett. **12**, 1333 (2012).
[64] K. J. Savage, M. M. Hawkeye, M. Matthew, R. Esteban, A. G. Borisov, J. Aizpurua, and J. J. Baumberg, Nature (London) **491**, 574 (2012).
[65] T. V. Teperik, P. Nordlander, J. Aizpurua, and A. G. Borisov, Phys. Rev. Lett. **110**, 263901 (2013).
[66] V. Kulkarni, E. Prodan, and P. Nordlader, Nano Lett. **13**, 5873 (2013).
[67] W. Q. Zhu, R. Esteban, A. G. Borisov, J. J. Baumberg, P. Nordlander, H. J. Lezec, J. Aizpurua, and K. B. Crozier, Nat. Commun. **7**, 11495 (2016).
[68] E. V. Chulkov, V. M. Silkin, and P. M. Echenique, Surf. Sci. **437**, 330 (1999).
[69] V. M. Silkin, A. García-Lekue, J. M. Pitarke, E. V. Chulkov, and P. M. Echenique, Europhys. Lett. **66**, 260 (2004).
[70] V. M. Silkin, J. M. Pitarke, E. V. Chulkov, and P. M. Echenique, Phys. Rev. B **72**, 115435 (2005).
[71] V. M. Silkin, T. Nagao, V. Despoja, J. P. Echeverry, S. V. Eremeev, E. V. Chulkov, and P. M. Echenique, Phys. Rev. B **84**, 165416 (2011).
[72] X. Zubizarreta, V. M. Silkin, and E. V. Chulkov, Phys. Rev. B **84**, 115144 (2011).
[73] X. Zubizarreta, V. M. Silkin, and E. V. Chulkov, Phys. Rev. B **87**, 115112 (2013).
[74] X. Zubizarreta, V. M. Silkin, and E. V. Chulkov, Phys. Rev. B **90**, 165121 (2014).
[75] M. Rocca, Surf. Sci. Rep. **22**, 1 (1995).
[76] B. Diaconescu, K. Pohl, L. Vattuone, L. Savio, P. Hofmann, V. M. Silkin, J. M. Pitarke, E. V. Chulkov, P. M. Echenique, and M. Rocca, Nature (London) **448**, 57 (2007).
[77] L. Vattuone, M. Smerieri, T. Langer, C. Tegenkamp, H. Pfnür, V. M. Silkin, E. V. Chulkov, P. M. Echenique, and M. Rocca, Phys. Rev. Lett. **110**, 127405 (2013).
[78] T. Eberlein, U. Bangert, R. R. Nair, R. Jones, M. Gass, A. L. Bleloch, K. S. Novoselov, A. Geim, and P. R. Briddon, Phys. Rev. B **77**, 233406 (2008).
[79] C. Kramberger, R. Hambach, C. Giorgetti, M. H. Rümmeli, M. Knupfer, J. Fink, B. Büchner, L. Reining, E. Einarsson, S. Maruyama, F. Sottile, K. Hannewald, V. Olevano, A. G. Marinopoulos, and T. Pichler, Phys. Rev. Lett. **100**, 196803 (2008).
[80] J. Yan, K. S. Thygesen, and K. W. Jacobsen, Phys. Rev. Lett. **106**, 146803 (2011).
[81] V. Despoja, K. Dekanić, M. Šunjić, and L. Marušić, Phys. Rev. B **86**, 165419 (2012).
[82] V. Despoja, D. Novko, K. Dekanić, M. Šunjić, and L. Marušić, Phys. Rev. B **87**, 075447 (2013).
[83] P. Wachsmuth, R. Hambach, M. K. Kinyanjui, M. Guzzo, G. Benner, and U. Kaiser, Phys. Rev. B **88**, 075433 (2013).
[84] F. J. Nelson, J.-C. Idrobo, J. D. Fite, Z. L. Miskovic, S. J. Pennycook, S. T. Pantelides, J. U. Lee, and A. C. Diebold, Nano Lett. **14**, 3827 (2014).
[85] M. Pisarra, A. Sindona, P. Riccardi, V. M. Silkin, and J. M. Pitarke, New J. Phys. **16**, 083003 (2014).
[86] S. C. Liou, C.-S. Shie, C. H. Chen, R. Breitwieser, W. W. Pai, G. Y. Guo, and M.-W. Chu, Phys. Rev. B **91**, 045418 (2015).
[87] D. Novko, V. Despoja, and M. Šunjić, Phys. Rev. B **91**, 195407 (2015).
[88] M. Pisarra, A. Sindona, M. Gravina, V. M. Silkin, and J. M. Pitarke, Phys. Rev. B **93**, 035440 (2016).

[89] D. Novko, M. Šunjić, and V. Despoja, Phys. Rev. B **93**, 125413 (2016).
[90] V. M. Silkin, B. Hellsing, L. Walldén, P. M. Echenique, and E. V. Chulkov, Phys. Rev. B **81**, 113406 (2010).
[91] V. M. Silkin, E. V. Chulkov, J. P. Echeverry, and P. M. Echenique, Phys. Stat. Sol. B **247**, 1849 (2010).
[92] B. N. J. Persson and E. Zaremba, Phys. Rev. B **31**, 1863 (1985).
[93] A. Liebsch, Phys. Scr. **35**, 354 (1987).
[94] E. Runge and E. K. U. Gross, Phys. Rev. Lett. **52**, 997 (1984).
[95] M. Petersilka, U. J. Gossmann, and E. K. U. Gross, Phys. Rev. Lett. **76**, 1212 (1996).
[96] K.-D. Tsuei, E. W. Plummer, A. Liebsch, E. Pehlke, K. Kempa, and P. Bakshi, Surf. Sci. **247**, 302 (1991).
[97] T. Nagao, in *Dynamics at Solid State Surfaces and Interfaces*, edited by U. Bovensiepen, H. Petek, and M. Wolf (Wiley VCH, Manheim, 2010), Vol. I, p. 189.
[98] T. Nagao, T. Hildebrandt, M. Henzler, and S. Hasegawa, Phys. Rev. Lett. **86**, 5747 (2001).
[99] F. Aryasetiawan and K. Karlsson, Phys. Rev. Lett. **73**, 1679 (1994).
[100] E. E. Krasovskii and W. Schattke, Phys. Rev. B **59**, R15609 (1999).
[101] H. Ishida and A. Liebsch, Phys. Rev. B **54**, 14127 (1996).
[102] K. Glantschnig and C. Ambrosch-Draxl, New J. Phys. **12**, 103048 (2010).
[103] V. P. Zhukov, F. Aryasetiawan, E. V. Chulkov, I. G. de Gurtubay, and P. M. Echenique, Phys. Rev. B **64**, 195122 (2001).
[104] V. M. Silkin, E. V. Chulkov, I. Y. Sklyadneva, and V. E. Panin, Izv. Vysch. Uchebn. Zaved. Fiz. **9**, 56 (1984) [Sov. Phys. J. **27**, 762 (1985)].
[105] G. B. Bachelet, D. R. Hamann, and M. Schlüter, Phys. Rev. B **26**, 4199 (1982).
[106] J. P. Perdew and A. Zunger, Phys. Rev. B **23**, 5048 (1981).
[107] D. M. Ceperley and B. J. Alder, Phys. Rev. Lett. **45**, 566 (1980).
[108] V. M. Silkin, E. V. Chulkov, and P. M. Echenique, Phys. Rev. B **68**, 205106 (2003).
[109] A. Bergara, V. M. Silkin, E. V. Chulkov, and P. M. Echenique, Phys. Rev. B **67**, 245402 (2003).
[110] V. U. Nazarov, New J. Phys. **17**, 073018 (2015).
[111] C. M. Wei and M. Y. Chou, Phys. Rev. B **66**, 233408 (2002).
[112] C. J. Powell, Proc. Phys. Soc. **76**, 593 (1960).
[113] M. Rocca, F. Biggio, and U. Valbusa, Phys. Rev. B **42**, 2835 (1990).
[114] M. Rocca, M. Lazzarino, and U. Valbusa, Phys. Rev. Lett. **69**, 2122 (1992).
[115] M. Rocca, L. Yibing, F. Buatier de Mongeot, and U. Valbusa, Phys. Rev. B **52**, 14947 (1995).
[116] F. H. L. Koppens, D. E. Chang, and F. J. Garcia de Abajo, Nano Lett. **11**, 3370 (2011).
[117] A. N. Grigirenko, M. Polini, and K. S. Novoselov, Nat. Photon. **6**, 749 (2012).
[118] F. J. Garcia de Abajo, ACS Photon. **1**, 135 (2014).